



Full observation of ultrafast cascaded radiationless transitions from $S_2(\pi\pi^*)$ state of pyrazine using vacuum ultraviolet photoelectron imaging

Cite as: J. Chem. Phys. **145**, 044306 (2016); <https://doi.org/10.1063/1.4955296>

Submitted: 01 April 2016 . Accepted: 23 June 2016 . Published Online: 25 July 2016

Takuya Horio, Roman Spesyvtsev , Kazuki Nagashima, Rebecca A. Ingle, Yoshi-ichi Suzuki, and Toshinori Suzuki 

COLLECTIONS

Paper published as part of the special topic on [Collection](#)



View Online



Export Citation



CrossMark

ARTICLES YOU MAY BE INTERESTED IN

[Ultrafast photodynamics of pyrazine in the vacuum ultraviolet region studied by time-resolved photoelectron imaging using 7.8-eV pulses](#)

The Journal of Chemical Physics **145**, 044307 (2016); <https://doi.org/10.1063/1.4955298>

[Real-time detection of \$S\(^1D_2\)\$ photofragments produced from the \$^1B_2\(^1\Sigma_u^+\)\$ state of \$CS_2\$ by vacuum ultraviolet photoelectron imaging using 133 nm probe pulses](#)

The Journal of Chemical Physics **147**, 013932 (2017); <https://doi.org/10.1063/1.4982219>

[Time-resolved photoelectron imaging of ultrafast \$S_2 \rightarrow S_1\$ internal conversion through conical intersection in pyrazine](#)

The Journal of Chemical Physics **132**, 174302 (2010); <https://doi.org/10.1063/1.3395206>

Lock-in Amplifiers
up to 600 MHz



Full observation of ultrafast cascaded radiationless transitions from $S_2(\pi\pi^*)$ state of pyrazine using vacuum ultraviolet photoelectron imaging

Takuya Horio, Roman Spesyvtsev,^{a)} Kazuki Nagashima, Rebecca A. Ingle,^{b)} Yoshi-ichi Suzuki,^{c)} and Toshinori Suzuki^{d)}

Department of Chemistry, Graduate School of Science, Kyoto University, Kitashirakawa Oiwake-cho, Sakyo-Ku, Kyoto 606-8502, Japan

(Received 1 April 2016; accepted 23 June 2016; published online 25 July 2016)

A photoexcited molecule undergoes multiple deactivation and reaction processes simultaneously or sequentially, which have been observed by combinations of various experimental methods. However, a single experimental method that enables complete observation of the photo-induced dynamics would be of great assistance for such studies. Here we report a full observation of cascaded electronic dephasing from $S_2(\pi\pi^*)$ in pyrazine ($C_4N_2H_4$) by time-resolved photoelectron imaging (TRPEI) using 9.3-eV vacuum ultraviolet pulses with a sub-20 fs time duration. While we previously demonstrated a real-time observation of the ultrafast $S_2(\pi\pi^*) \rightarrow S_1(n\pi^*)$ internal conversion in pyrazine using TRPEI with UV pulses, this study presents a complete observation of the dynamics including radiationless transitions from S_1 to S_0 (internal conversion) and $T_1(n\pi^*)$ (intersystem crossing). Also discussed are the role of ${}^1A_u(n\pi^*)$ in the internal conversion and the configuration interaction of the $S_2(\pi\pi^*)$ electronic wave function. *Published by AIP Publishing.* [<http://dx.doi.org/10.1063/1.4955296>]

I. INTRODUCTION

A photoexcited molecule undergoes a variety of photophysical and photochemical processes, which have been studied using combinations of various experimental methods. In general, each method enables observation of only a part of the dynamics such as internal conversion (IC), intersystem crossing (ISC), or dissociation, and it is usually difficult to elucidate the entire dynamics with a single experimental method. Time-resolved photoelectron spectroscopy (TRPES)^{1,2} or time-resolved photoelectron imaging (TRPEI)³ can potentially capture the complete photo-induced dynamics because photoionization can be induced from any part of the potential energy surfaces (PESs) involved. However, such “universal” photoionization detection requires ultrashort pulses with sufficiently high photon energies, namely, in the vacuum UV (VUV) region, to enable photoionization from low-lying excited states and the ground state, which has been technically difficult. Filamentation four-wave mixing using a windowless gas cell⁴ enables routine generation of sub-20 fs VUV pulses without propagation through a narrow hollow fiber or dispersion compensation, and it significantly reduced technical complexities associated with ultrafast spectroscopy in the VUV region. Here we demonstrate TRPEI using intense 9.3-eV VUV pulses with a sub-20 fs time duration,⁵ generated

by filamentation four-wave mixing, as an experimental method to observe the entire photo-induced dynamics of a large polyatomic molecule. We apply this method to the benchmark system of pyrazine ($C_4N_2H_4$) and critically test its performance.

Conical intersections (CIs) of PESs facilitate ultrafast IC, and they play crucial roles in the photostability of nucleobases,^{6,7} the primary process in vision,⁸ and photochromic reactions.⁹ Much experimental effort^{8,10} has been devoted to the direct observation of IC via CIs in the recent years. The ultrafast IC from the $S_2(\pi\pi^*, {}^1B_{2u})$ state of pyrazine to the $S_1(n\pi^*, {}^1B_{3u})$ state via a CI is one of the best-known systems in these studies.¹¹ Since the pioneering theoretical study by Domcke and co-workers on the S_2/S_1 CI of pyrazine using *ab initio* calculations,¹² a number of theoretical studies^{13–23} predicted a broad $S_2 \leftarrow S_0$ photoabsorption spectrum²⁴ (230–270 nm), consistent with the picture of ultrafast IC via CI.

Since the Franck-Condon region in the S_2 state of pyrazine is very close to the S_2/S_1 CI, IC occurs within one vibrational period (<30 fs). Therefore, real-time observation of IC requires an extremely high time resolution. Using a sub-20 fs deep-UV (264 and 198 nm) light source,²⁵ the $S_2(\pi\pi^*) \rightarrow S_1(n\pi^*)$ IC was clearly observed for the first time in our previous TRPEI²⁶ study; the S_2 lifetime limited by IC was determined to be 22 ± 3 fs.²⁷ Earlier TRPEI²⁸ and TRPES²⁹ studies carried out in the 1990s were unable to observe the $S_2(\pi\pi^*) \rightarrow S_1(n\pi^*)$ IC in real time due to insufficient time resolution, and they reported the lifetimes of vibrationally excited S_1 state populated from S_2 to be 17.5–22 ps.^{28,29} However, it is important that the S_1 state populated by IC from S_2 is short-lived and it undergoes further dynamics, which have not been fully elucidated.

^{a)}Present address: SUPA, School of Physics and Astronomy, University of St. Andrews, North Haugh, St. Andrews, Fife KY16 9SS, United Kingdom.

^{b)}Permanent address: School of Chemistry, University of Bristol, Cantock's Close, Bristol BS8 1TS, United Kingdom.

^{c)}Present address: Faculty of Pharmaceutical Science, Health Sciences University of Hokkaido, Ishikari-Tobetsu, Hokkaido 061-0293, Japan.

^{d)}Author to whom correspondence should be addressed. Electronic mail: suzuki@kuchem.kyoto-u.ac.jp

The $S_1(n\pi^*)$ state of pyrazine is a well-known intermediate coupling case of radiationless transition,^{30,31} and the S_1 lifetime at the zero vibrational level (origin) is as short as 110 ps.²⁴ ISC from the S_1 origin has been observed by TRPEI using a 200 nm probe pulse,³² a 58.4 nm probe pulse generated by a VUV free electron laser,³³ or a visible pulse using two-photon ionization via Rydberg states.³⁴ The ISC quantum yield, Φ_{ISC} , to T_1 was shown by Yamazaki *et al.*²⁴ to be almost unity at the origin of S_1 , while it diminishes as the excess vibrational energy in S_1 increases; however, they have also shown that Φ_{ISC} around the S_2 origin (264 nm) is still as large as 0.13. Therefore, ISC occurs from the vibrationally hot S_1 state produced by ultrafast IC from S_2 . Furthermore, according to the same authors,²⁴ a quenching process other than ISC, which is most likely $S_1 \rightarrow S_0$ IC, has a larger quantum yield of 0.87. Although we have performed TRPEI using 161-nm probe pulses generated by a VUV free electron laser³⁵ or 159-nm pulses by filamentation four-wave mixing (accompanying paper⁶⁰), their photon energies were insufficient to detect the hot S_0 state. In this study, we observe the entire ultrafast electronic dephasing process including IC to S_0 of this benchmark system.

A new problem raised by recent theoretical studies on IC from $S_2(\pi\pi^*)$ is the role of the $^1A_u(n\pi^*)$ state.^{36–38} Previous on-the-fly surface hopping trajectory calculations based on time-dependent density functional theory²² suggested that the $^1A_u(n\pi^*)$ state plays some roles in the $S_2(\pi\pi^*) \rightarrow S_1(n\pi^*)$ IC. However, more recent quantum dynamics simulations by Sala *et al.*^{36,37} using PESs obtained by the extended multiconfiguration quasi-degenerate second order perturbation theory predicted that IC from $S_2(\pi\pi^*)$ bifurcates into $^1A_u(n\pi^*)$ and $S_1(n\pi^*)$ with almost equal branching ratios. On the other hand, quantum dynamical calculations using PESs obtained by the multireference configuration interaction (MRCI) method³⁸ claimed that the non-adiabatic transition probability from $S_2(\pi\pi^*)$ to $^1A_u(n\pi^*)$ is vanishingly small, supporting the conventional two-state picture of $S_2(\pi\pi^*) \rightarrow S_1(n\pi^*)$. Thus, we examine any evidence for IC to $^1A_u(n\pi^*)$ in this paper.

One of the basic ideas in TRPES and TRPEI is to explore the time evolution of a non-stationary electronic wave function by projecting it to cationic electronic states; the time-evolving partial ionization cross sections should reveal variations in the electronic character of the ionized state. However, this idea has not been fully exploited owing to the lack of a convenient VUV ultrafast laser. One of the few exceptions was the study by Schmitt *et al.*,³⁹ who employed molecules with low ionization energies and a deep-UV laser. Alternatively, we have previously employed time-evolving photoelectron angular distributions (PADs) or differential ionization cross sections to probe the electron configuration.^{26,40} Here we employ partial ionization cross sections to different cationic states and investigate configuration interaction in the excited electronic states.

II. EXPERIMENTAL METHOD

The experimental setup has been described in detail in our previous reports.^{4,5} Briefly, a cryogenically cooled Ti:sapphire

multipass amplifier generated 25 fs, 1.7 mJ, 770 nm pulses at a 1 kHz repetition rate. The fundamental pulse (ω) was split into two beams in a ratio of 70:30. The higher intensity beam was converted to the second harmonic (2ω) using a β -BBO crystal (0.3 mm thickness), and then gently focused with a dichroic concave mirror ($r = -2000$ mm) into a neon gas cell through a Brewster-angled CaF_2 window (1 mm thickness). The 30% portion of the fundamental beam was also focused into the same gas cell with another dichroic concave mirror ($r = -2000$ mm) and collinearly overlapped with the 2ω beam using a beam combiner. Just prior to the entrance window of the gas cell, the pulse energies of the ω and 2ω beams were 0.48 and 0.42 mJ/pulse, respectively. The spatiotemporal overlap between the ω and 2ω beams was carefully adjusted in order to initiate filamentation four-wave mixing for frequency up-conversion. The pressure in the neon gas cell was maintained at about 250 Torr. The gas cell was connected to a multi-stage differential pumping system equipped with a laser-drilled pinhole ($\sim\varnothing 0.3$ mm), a narrow channel (1.25 mm in diameter and 20 mm in length), and an aperture ($\varnothing 3$ mm) to reduce the gas conductance between the cell and an adjacent optics chamber held under high-vacuum (10^{-6} Torr).

As reported previously,^{4,5} 3ω (4.7 eV), 4ω (6.3 eV), 5ω (7.8 eV), and 6ω (9.3 eV) are generated simultaneously from various four-wave mixing processes in the neon filament. These output beams propagate collinearly with the primary beams (ω and 2ω) through the differential pumping system and enter the high-vacuum chamber, which houses a translational delay stage and several mirrors for separation and recombination of the pump (3ω) and probe (6ω) pulses. A UV-enhanced aluminum mirror with a $\varnothing 3$ mm aperture was used to spatially separate the central and peripheral regions of the output beam. The central portion passed through the aperture and was then reflected with five dichroic mirrors designed for 6ω to remove the other colors (ω , 2ω , 3ω , 4ω , and 5ω). The peripheral portion was reflected from the holed mirror and underwent four additional reflections from dichroic mirrors designed for 3ω to isolate the 3ω component from the other colors (ω , 2ω , 4ω , 5ω , and 6ω). The purified 3ω and 6ω beams were finally focused with separate concave mirrors (both $r = -1000$ mm) on a molecular beam of pyrazine (<1%) seeded in helium carrier gas. Two of the dichroic mirrors in the 6ω optical train were mounted to a vacuum-compatible, motorized translation stage so that the timing of the 6ω probe pulse with respect to the 3ω pump pulse could be controlled. The on-target pulse energies of 3ω and 6ω were estimated to be ~ 500 nJ/pulse and ~ 5 nJ/pulse, respectively.

Our photoelectron imaging apparatus employs a doubly skimmed molecular beam supplied by a water-cooled Even-Lavie pulsed valve.⁴¹ The pulsed valve was operated at 1 kHz and the timing between the pulsed molecular beam and the femtosecond laser pulses was optimized with a digital pulse generator. Photoelectrons generated with the 3ω and 6ω pulses were accelerated through an electrostatic lens system operated in a velocity mapping mode⁴² and projected onto a dual microchannel plate (MCP, $\varnothing 75$ mm effective area) backed by a phosphor screen (P46). The polarization vectors of both laser beams were aligned parallel to each other and also set parallel to the MCP detector surface. Projected images of the

photoelectrons were obtained as a function of the pump-probe delay time for short delays (-47 to $+49$ fs), intermediate delays (-110 to $+230$ fs), and long delays (1 – 80 ps).

The projected images were recorded with an image-intensified CCD camera (1024×1024 pixels) and analyzed using the p-BASEX algorithm⁴³ to obtain time-dependent photoelectron kinetic energy (PKE) and angular distributions. Since photoelectrons due to one-photon ionization with the 6ω pulses, two/three-photon ionization with the 3ω pulses, and secondary electrons from the acceleration electrodes result in time-independent background signal, such background contributions were subtracted prior to the inversion. The time origin for the pump-probe delay was determined using a cross correlation trace measured by non-resonant $(1 + 1')$ multiphoton ionization of krypton. The trace could be fitted using a single Gaussian with a full width at half maximum (FWHM) of 25 fs. The PKE was calibrated using one-color three-photon ionization of xenon with the 3ω pulses.

Setting the polarity of the acceleration electrodes to positive, we also examined time-of-flight (TOF) mass spectra of photoions. Since the photon energy of 6ω (9.3 eV) is only slightly larger than the adiabatic ionization energy of pyrazine (9.288 eV),⁴⁴ only parent ions of pyrazine ($m/e = 80$) were observed in the TOF-mass spectra. On the other hand, three-photon ionization of pyrazine with 3ω pulses (total photon energy of ~ 14 eV) yielded fragment ions at $m/e = 53$ and 26, which were also observed in our previous study.⁴⁴ No signals were observed for both pyrazine clusters and a pyrazine-helium complex in the TOF mass spectra.

Fig. 1(a) shows a schematic diagram of the 3ω pump and 6ω probe experiment, namely, the $(1 + 1')$ resonance-enhanced multiphoton ionization (REMPI) scheme. In this study, we also performed an additional experiment using $(1 + 2')$ REMPI (Fig. 1(b)). As will be shown later, the $(1 + 2')$ REMPI scheme enabled us to confirm $S_1(n\pi^*) \rightarrow T_1(n\pi^*)$ ISC. In the $(1 + 2')$ REMPI experiment, we employed two optical parametric amplifiers (OPAs) and varied the wavelength of the pump pulse, ω_1 , from 270 to 244 nm, while

the wavelength for the probe pulse, ω_2 , was fixed at 358 nm. The typical pulse energies for ω_1 and ω_2 were adjusted to be ~ 0.3 and ~ 6 $\mu\text{J}/\text{pulse}$, respectively. The PKE calibration was performed using four-photon ionization of xenon with ω_2 (358 nm) pulses.

III. RESULTS AND DISCUSSION

A. S_2/S_1 internal conversion dynamics

Figure 2 presents representative snapshots of the two-dimensional (2D) slice through the three-dimensional (3D) photoelectron scattering distribution observed at short time delays. The images observed at 1 and 25 fs are noticeably different, reflecting the influence of ultrafast IC from $S_2(n\pi^*)$.

From a series of such photoelectron images, we constructed 2D maps of the photoelectron kinetic energy distributions (PKEDs) versus the delay time for short (-47 to $+49$ fs) and long (1 – 80 ps) pump-probe delays. We discuss short delay times first and then long delay times in Section III C. Figure 3(a) presents the time-energy 2D map for delay times of -47 to $+49$ fs. One of the most striking features is the photoelectron signal in the PKE region of 1.5–2.5 eV, which was not observed in our previous study using a 4ω probe pulse.²⁷ For a closer examination of this feature, Figure 4 shows PKEDs obtained for delay times from 1 to 49 fs. The signal in the 1.5–2.5 eV region appears immediately after the 3ω pump pulse, shifts progressively to lower energy, and vanishes by 25 fs, which is in excellent agreement with the S_2 lifetime of 22 fs determined by our previous study.²⁷ As we explain in more detail below, this feature manifests the nuclear

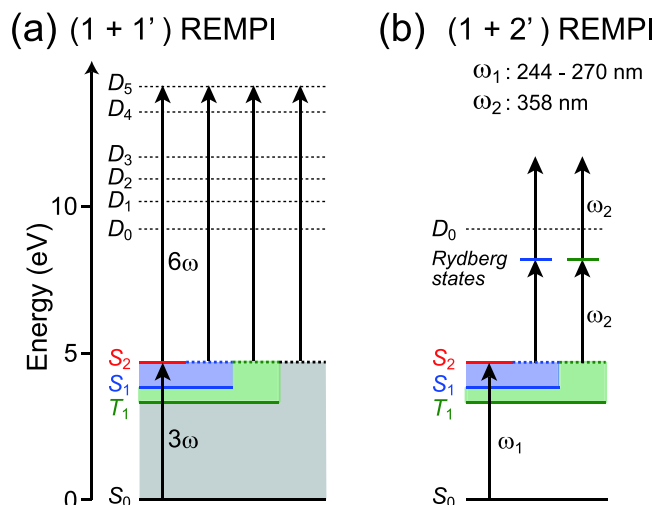


FIG. 1. Schematic diagrams of (a) $(1 + 1')$ REMPI using 3ω and 6ω pulses and (b) $(1 + 2')$ REMPI using ω_1 (244–270 nm) and ω_2 (358 nm) pulses.

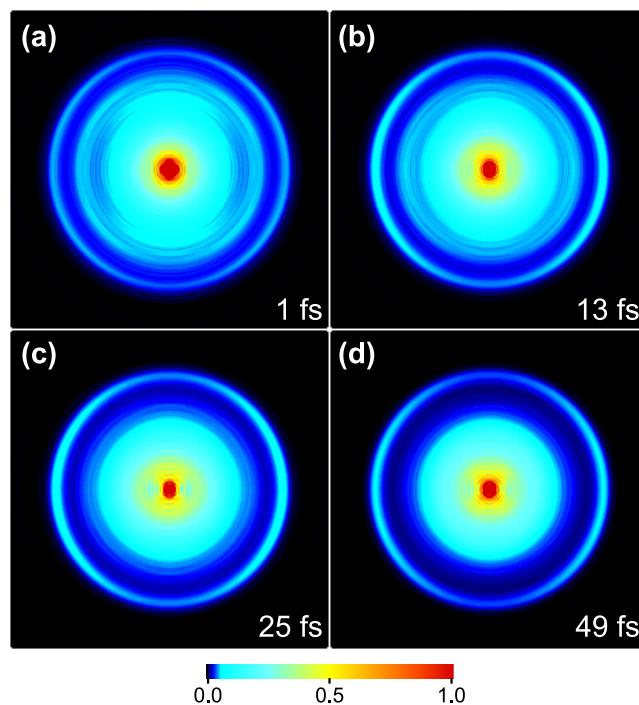


FIG. 2. 2D slices through the 3D photoelectron scattering distributions obtained at (a) 1, (b) 13, (c) 25, and (d) 49 fs. The directions of the polarization vectors of the 3ω and 6ω pulses are parallel to each other and vertical in the plane of the figure.

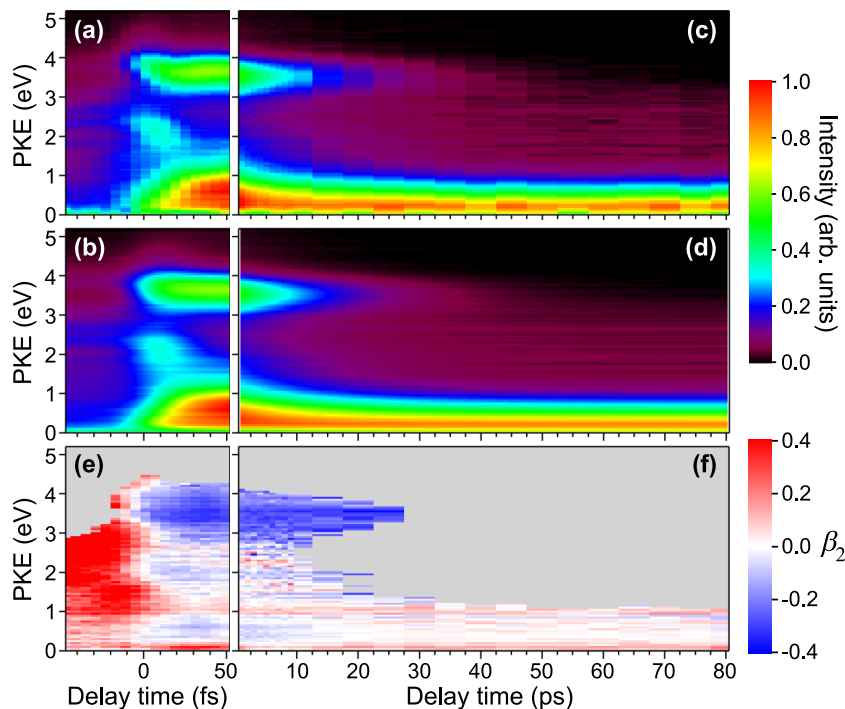


FIG. 3. (a) Measured and (b) fitted time-dependent photoelectron kinetic energy distributions from -47 to 49 fs. (c) Measured and (d) fitted time-dependent photoelectron kinetic energy distributions from 1 to 80 ps. Time-dependent photoelectron anisotropy parameter, β_2 , for delay times of (e) -47 to 49 fs and (f) 1 – 80 ps. The β_2 values are displayed only in the regions where the normalized photoelectron intensities in (a) and (c) are greater than 0.1 .

wavepacket motion from the S_2 Franck-Condon region to the S_2/S_1 CI.

For a quantitative analysis, we fit the 2D map shown in Fig. 3(a) using a kinetic model that employs an exponential decay component, $C_{\text{decay}}(E) \times [\exp(-t/\tau_2)]$, and an exponential rise component, $C_{\text{rise}}(E) \times [1 - \exp(-t/\tau_2)]$, where E denotes the PKE. The time constant, τ_2 , corresponds to the S_2 lifetime, which was determined to be 22 fs from a global fit in our previous study using 4ω probe pulses.²⁷ An exponential decay component, $C_{\text{nt}}(E) \times [\exp(t/\tau_{\text{nt}})]$, was also included in the model for negative delay times because weak “probe-pump” signals appeared in that region. Since the negative-time signal does not exhibit a noticeable decay in intensity in the observation window, the time constant, τ_{nt} , did not affect the quality of our fitting for positive delay times. Thus, τ_{nt} was set to a large value of 300 fs. A Gaussian distribution with a FWHM of 25 fs was also employed as a

cross correlation function in the fitting process. Consequently, the parameters to fit were the coefficients $C_{\text{decay}}(E)$, $C_{\text{rise}}(E)$, and $C_{\text{nt}}(E)$ at each PKE subsection (0.05 eV), and these were determined by least squares fitting using the Levenberg-Marquardt algorithm. The fitting results are presented in Fig. 3(b), which capture the overall features of the observed 2D map shown in Fig. 3(a).

After the signal due to the short-lived S_2 state disappears, two bands remain in the PKE regions of 3 – 4 and 0 – 1.5 eV, as can be seen in Figs. 3(a) and 3(b). The fitting result shown in Fig. 3(b) ensures that both of these bands are well explained by the rise time constant of 22 fs, which means that they are due to photoionization from the vibrationally hot S_1 state populated by IC. The 3 – 4 eV component is unambiguously assigned as photoionization signal of $D_0(n^{-1}) \leftarrow S_1(n\pi^*)$, because the corresponding band appeared in the energy region of 0 – 1 eV in our previous experiment using a 4ω probe pulse²⁷ and the observed PKE shift corresponds to the photon energy difference (~ 3 eV) between 4ω and 6ω .

Recently, IC from $S_2(\pi\pi^*)$ to ${}^1A_u(n\pi^*)$ was predicted by theoretical calculations by Sala *et al.*^{36,37} Although the electronic energy of ${}^1A_u(n\pi^*)$ is not established yet, a number of electronic structure calculations predict that ${}^1A_u(n\pi^*)$ lies above $S_1(n\pi^*)$ at the equilibrium geometry in S_0 .^{37,38,45} Since configuration interaction calculations⁴⁶ showed that ${}^1A_u(n\pi^*)$ has a single leading configuration of $(6a_g)^{-1}(1a_u)^{+1}$ (one electron in the $6a_g$ orbital is promoted to the $1a_u$ orbital), photoionization is allowed from ${}^1A_u(n\pi^*)$ to $D_0(n^{-1})$ in terms of Koopmans’ correlation. Even if some geometrical changes are taken into account between ${}^1A_u(n\pi^*)$ and $D_0(n^{-1})$, PKE is expected to be greater for $D_0(n^{-1}) \leftarrow {}^1A_u(n\pi^*)$ than $D_0(n^{-1}) \leftarrow S_1(n\pi^*)$. As seen in the PKED in Fig. 4, no additional band appears in the PKE region higher than the $D_0(n^{-1}) \leftarrow S_1(n\pi^*)$ band. Thus, no signature of ${}^1A_u(n\pi^*)$ was detectable in the present study.

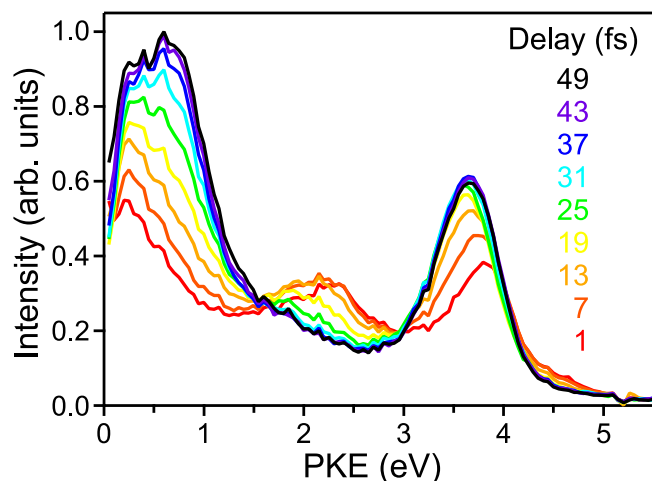


FIG. 4. PKEDs obtained for delay times from 1 to 49 fs.

If the quantum yield of $S_2 \rightarrow S_1$ IC is unity, isosbestic points should appear in time-dependent PKEDs. The pump pulse employed in the present study has a ~ 18 fs time duration, so that 96.1% of photoexcitation is completed within 13 fs. Close examination of PKEDs after 13 fs reveals two isosbestic points at 1.5 and 3.0 eV, which strongly suggests that IC from S_2 occurs predominantly to S_1 .

B. Configuration interaction of S_2 electronic wave function

The fitting result shown in Fig. 3(b) enabled us to extract the “time-averaged” PKED for S_2 , $C_{S_2}(E)$, which is presented with open squares in Fig. 5(a); note that $C_{S_2}(E)$ is identical to the coefficient, $C_{\text{decay}}(E)$. As can be seen in the figure, $C_{S_2}(E)$ exhibits multiple bands in the PKE region of 0–5.5 eV. In order to decompose $C_{S_2}(E)$ into each component, we performed multi-peak fitting assuming four bands. As observed in Figs. 3(a) and 4, the two components in the PKE regions of 1.5–2.5 and 3.2–4.2 eV shift to lower PKEs owing

to nuclear wavepacket motions from the S_2 Franck-Condon region to the S_2/S_1 CI. Thus, we employed exponential functions convoluted with Gaussian functions in order to account for such a dynamical effect. Gaussian functions were employed for the remaining two components, the band at ~ 0.3 eV and the high-energy tail of the 3.2–4.2 eV component. Hereafter, the former and latter components are referred to as the lowest and highest PKE components, respectively.

The result of the multi-peak fitting, shown with a solid line in Fig. 5(a), well reproduces $C_{S_2}(E)$. Using the total photon energy (14.0 eV) of the present pump-probe scheme and the adiabatic ionization energies of the cationic states of pyrazine,^{44,47} the largest possible PKEs, E_i^{max} , can be calculated for each cationic state, D_i . The calculated values of E_0^{max} , E_1^{max} , and E_3^{max} , represented by dashed vertical lines in Fig. 5(a), indicate that the highest PKE, 3.2–4.2 eV, and 1.5–2.5 eV components can be assigned as photoionization signals from S_2 into D_0 , D_1 , and D_3 , respectively. In fact, the $D_0 \leftarrow S_2$ and $D_1 \leftarrow S_2$ photoionization processes were identified in our previous study using 4ω probe pulses,²⁷ while the $D_3 \leftarrow S_2$ photoionization process was not observed due to the insufficient probe photon energy. As can be seen in Figs. 3(a) and 4, the PKED for $D_1 \leftarrow S_2$ energetically overlaps with that for $D_0 \leftarrow S_1$, while the PKED for $D_3 \leftarrow S_2$ is less affected by interference from photoionization signals from S_1 . Consequently, the $D_3 \leftarrow S_2$ signal is more spectrally isolated than that of $D_1 \leftarrow S_2$; therefore, nuclear wavepacket motion from the S_2 Franck-Condon region to the S_2/S_1 CI was more clearly observed from the former.

The configuration interaction study of $S_2(^1B_{2u})$ by Hackmeyer and Whitten⁴⁶ revealed that the $S_2(^1B_{2u})$ electronic wave function can be expressed with two leading configurations,

$$\Psi_{S_2} = 0.70 \times \Phi \left[(1b_{1g})^{-1} (2b_{3u})^{+1} \right] + 0.54 \times \Phi \left[(1b_{2g})^{-1} (1a_u)^{+1} \right]. \quad (1)$$

Nearly identical coefficients, 0.69 and 0.45, were respectively obtained for $\Phi[(1b_{1g})^{-1}(2b_{3u})^{+1}]$ and $\Phi[(1b_{2g})^{-1}(1a_u)^{+1}]$ in the recent MRCI calculation by Kanno *et al.*³⁸ As schematically presented in Fig. 5(b), $\Phi[(1b_{1g})^{-1}(2b_{3u})^{+1}]$ and $\Phi[(1b_{2g})^{-1}(1a_u)^{+1}]$ are electronically correlated with D_1 and D_3 , respectively. Therefore, the $D_1 \leftarrow S_2$ and $D_3 \leftarrow S_2$ photoionization processes are allowed in terms of Koopmans’ correlation, which qualitatively accounts for their large contributions in $C_{S_2}(E)$. Note that D_1 and D_3 have single leading configurations, $(1b_{1g})^{-1}$ and $(1b_{2g})^{-1}$, respectively.^{48–50} The present study enabled evaluation of the relative photoionization cross section between $D_1 \leftarrow S_2$ and $D_3 \leftarrow S_2$ processes and, therefore, quantitative examination of configuration interaction in the S_2 electronic wave function.

As shown in Fig. 5(a), the contribution of the $D_0 \leftarrow S_2$ process (the highest PKE component) is minor, so this process is ascribed as configuration interaction in S_2 and/or D_0 with small coefficients in their configuration functions. On the other hand, the contribution of the lowest PKE component is significant, and thus it should be assigned as an “allowed” photoionization process. According

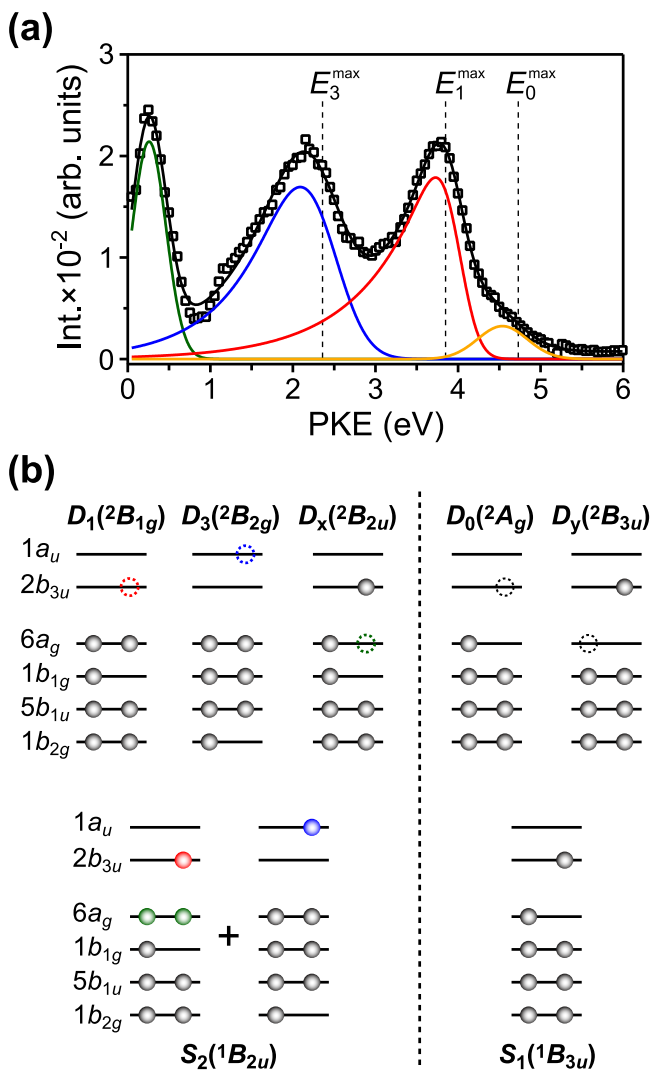


FIG. 5. (a) $C_{\text{decay}}(E)$ obtained from the fitting result shown in Fig. 3(b), which can be regarded as PKED for the short-lived S_2 state, $C_{S_2}(E)$. (b) The leading configurations for S_1 , S_2 , D_0 , D_1 , D_3 , D_x , and D_y (see main text).

to a high-resolution He(I) photoelectron spectrum⁴⁷ and theoretical calculations for pyrazine cation,^{48–50} six cationic states are energetically accessible in the present pump-probe study. These electronic states are $D_0(^2A_g)$, $D_1(^2B_{1g})$, $D_2(^2B_{1u})$, $D_3(^2B_{2g})$, $D_4(^2B_{3g})$, and $D_5(^2B_{3u})$, which have leading configurations of $(6a_g)^{-1}$, $(1b_{1g})^{-1}$, $(5b_{1u})^{-1}$, $(1b_{2g})^{-1}$, $(3b_{3g})^{-1}$, and $(1b_{3u})^{-1}$, respectively. However, only D_1 and D_3 are accessible from S_2 due to their electron configurations, as presented in Fig. 5(b). *Ab initio* MRCI calculations for pyrazine cation⁵¹ predicted a cationic state with a leading configuration of $(1b_{1g})^{-1}(6a_g)^{-1}(2b_{3u})^+1$ at 13.31 eV above S_0 . This ionic state, which we denote as D_x (see Fig. 5(b)), has not been detected experimentally because one-photon ionization from S_0 into D_x is forbidden in terms of Koopmans' correlation. On the other hand, as shown in Fig. 5(b), $D_x \leftarrow S_2$ photoionization is allowed; an electron in the $6a_g$ orbital of the $\Phi[(1b_{1g})^{-1}(2b_{3u})^+1]$ component in S_2 is ejected by the 6ω probe, leaving $2b_{3u}$ as a singly occupied molecular orbital (SOMO). Thus, the lowest PKE component shown in Fig. 5(a) is assigned as $D_x \leftarrow S_2$ photoionization signal.

As demonstrated in Fig. 5(a), the present study has revealed configuration interaction in an electronic excited state of a molecule. A similar result has been reported by Schmitt *et al.*,³⁹ who investigated phenanthrene, which has small ionization energies of D_0 (7.89 eV), D_1 (8.44 eV), and D_2 (9.27 eV), and discussed configuration interaction in S_2 (4.39 eV) and S_1 (3.64 eV) using photoionization with 207.5 nm (5.98 eV) pulses. It is worth noting that a 6ω VUV probe (9.3 eV) can be applied to a broader range of molecules.

C. Cascaded radiationless transitions from vibrationally hot S_1

In our previous investigation using a 4ω probe,²⁷ we observed the vibrational quantum beats of the ν_{6a} mode (583 cm^{-1})⁵² for $S_1(n\pi^*)$. In this study, we investigated the beats using the 6ω probe. Figure 6(a) presents a blowup of the

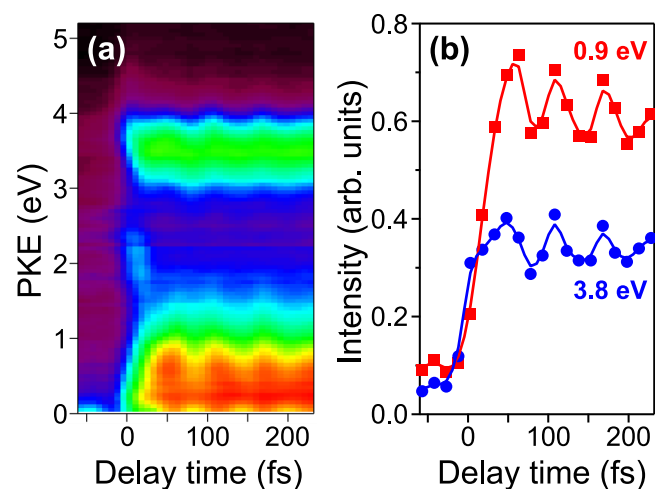
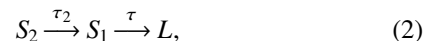


FIG. 6. (a) 2D map of time-dependent photoelectron kinetic energy distributions from -110 to 230 fs. (b) PKE-resolved time profiles at 0.9 and 3.8 eV obtained from the 2D map. The time profiles with 15 fs intervals are plotted with circles, while the interpolated ones (7.5 fs intervals) are plotted with solid lines.

time-energy map for -110 to $+230$ fs delay times. The images were taken at 15 fs intervals in the delay time; however, in order to present the vibrational quantum beat more clearly, the 2D map shown in Fig. 6(a) was interpolated using a cubic spline such that the intervals are 7.5 fs. As can be seen in Fig. 6(a), the quantum beats are obvious for the two components appearing in the PKE regions of $3\text{--}4$ and $0\text{--}1.5$ eV. Signal intensities obtained at 0.9 (squares) and 3.8 eV (circles) are presented in Figure 6(b). The intensities of the two signals oscillate in phase with a period of approximately 60 fs, which corresponds to one period of the ν_{6a} vibrational mode in $S_1(n\pi^*)$. This result indicates that the $0\text{--}1.5$ eV component is also due to photoionization from $S_1(n\pi^*)$.

To further investigate the two bands for much longer time delays, we measured photoelectron images from 1 to 80 ps (the maximum delay time in the present experiment). Representative photoelectron images measured at delay times of 1 , 10 , 40 , and 80 ps are shown in Fig. 7, and a 2D map of PKEDs constructed from a series of the observed images is presented in Fig. 3(c).

As can be seen in Fig. 3(c), while the 2D map exhibits a long-lived (>80 ps) component in the PKE region of $0\text{--}1$ eV, the intensity in the $3\text{--}4$ eV region decays in less than 20 ps. Thus, we assumed the following sequential relaxation processes in order to perform a global fitting of the time-energy map shown in Fig. 3(c) for the long time delays:



where τ_2 is the S_2 lifetime (22 fs, as mentioned above), τ is the S_1 lifetime, and L denotes any long-lived state(s). The 2D

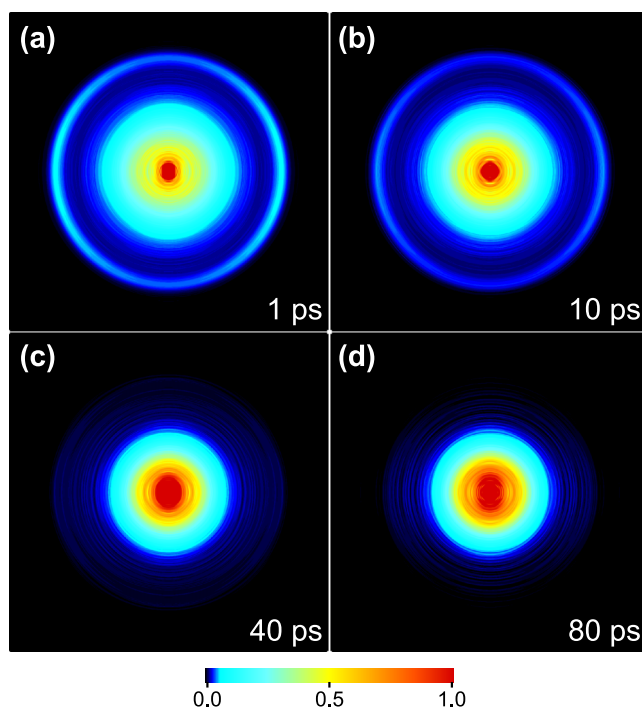


FIG. 7. 2D slices of the 3D photoelectron scattering distributions obtained at (a) 1 , (b) 10 , (c) 40 , and (d) 80 ps. The directions of the polarization vectors of the 3ω and 6ω pulses are parallel to each other and vertical in the plane of the figure.

map of PKEDs, $I(E, t)$, is thus expressed as

$$I(E, t) = \{C_{S_2}(E)[S_2(t)] + C_{S_1}(E)[S_1(t)] + C_L(E)[L(t)]\} \otimes g(t), \quad (3)$$

where the coefficients $C_{S_2}(E)$, $C_{S_1}(E)$, and $C_L(E)$ are PKEDs for S_2 , S_1 , and L , respectively, and $g(t)$ is the cross correlation function. An explicit analytical formula for Eq. (3) is given in the supplementary material.⁵³ Note that because there is no contribution from the S_2 state after 1 ps, the global fitting was performed without including it. The result of the global fitting is presented in Fig. 3(d), which well reproduces the observed 2D map shown in Fig. 3(c). The lifetime of τ was determined to be 14.8 ± 0.1 ps, where the uncertainty corresponds to one standard deviation in the global fit. This value is in fair agreement with, but clearly shorter than, the values of 17.5–22 ps obtained at the excitation wavelengths around the S_2 origin (264 nm).^{24,28,29} This is ascribed to the broadband spectrum of our 3ω pump pulse⁴ employed in the present study. As will be shown later, when the lifetime is measured using a longer pulse duration of 100–200 fs with a narrower spectral bandwidth, the pump wavelength dependence of the lifetime is clearly observed (see Fig. 10(b)).

A comparison of $C_{S_1}(E)$ and $C_L(E)$ obtained by the global fit is presented in Fig. 8(a). The former can be divided into two components appearing in the PKE regions of 3–4 and 0–1.5 eV. As mentioned above, the 3–4 eV band is assigned as $D_0(n^{-1}) \leftarrow S_1(n\pi^*)$ photoionization signal. According to configuration interaction calculations of the electronic ground and excited states of pyrazine,⁴⁶ $S_1(n\pi^*)$ has a leading configuration of $(6a_g)^{-1}(2b_{3u})^{+1}$. Thus, photoionization from $S_1(n\pi^*)$ into $D_0(n^{-1})$ is allowed in terms of Koopmans' correlation (see Fig. 5(b)). Since the 0–1.5 eV component of $C_{S_1}(E)$ exhibits a strong photoionization signal (see Fig. 8(a)), it is likely that this component also originates from an allowed photoionization process. In the same manner as the $D_x \leftarrow S_2$ photoionization process, the 0–1.5 eV component

is assigned as $D_y \leftarrow S_1$ photoionization signal, as presented in Fig. 5(b). D_y , which has a single leading configuration of $(6a_g)^{-2}(2b_{3u})^{+1}$ is calculated to be 12.58 eV above S_0 by *ab initio* MRCI calculations.⁵¹ It is noted that if the $S_1 \leftarrow S_0$ and $D_y \leftarrow D_0$ excitation energies are similar, the photoelectron signals for the $D_0 \leftarrow S_0$ and $D_y \leftarrow S_1$ processes energetically overlap in PKE. In other words, when an independent orbital approximation and Koopmans' theorem are valid, the electron binding energy (eBE) of a given orbital is independent of the occupancies of other orbitals. Consequently, it is anticipated that photoionization from the same orbital appears at a similar eBE in the experiment. When they appear at exactly the same eBE, the method may be regarded as MO-sensitive spectroscopy; however, the independent orbital approximation is crude, so that the observed eBEs are generally different.

The PKED for the long-lived state, $C_L(E)$, shown in Fig. 8(a) exhibits an intense band in the PKE region of 0–1 eV. A possible candidate for the long-lived state appearing at 0–1 eV is the electronic ground state, $S_0(1A_g)$, or the triplet excited state, $T_1(n\pi^*, {}^3B_{3u})$. The former dissociates into HCN + C_3NH_3 on the microsecond time scale⁵⁴ and the latter has a nanosecond lifetime.⁵⁵

To assign the 0–1 eV component, we extracted the photoelectron anisotropy parameter, β_2 , defined by the laboratory-frame photoelectron angular distribution,

$$I(E, \theta, t) = \frac{\sigma(E, t)}{4\pi} [1 + \beta_2(E, t)P_2(\cos \theta) + \beta_4(E, t)P_4(\cos \theta)], \quad (4)$$

where E , θ , and t , respectively, denote PKE, the ejection angle of photoelectrons with respect to the laser polarization and the delay time, and $P_n(\cos \theta)$ is an n th order Legendre polynomial. Figure 8(b) presents β_2 parameters as a function of PKE obtained by averaging the β_2 values from 50 to 80 ps, which is the time range when S_1 has already decayed and the contributions from the $D_0 \leftarrow S_1$ and $D_y \leftarrow S_1$ signals are negligible. The most robust feature of Fig. 8(b) is that β_2 is almost zero without any noticeable PKE dependence between 0 and 1 eV. Since the β_2 values for $D_0 \leftarrow S_1$, namely, photoionization from the $\pi^*(2b_{3u})$ orbital, exhibit a strong negative dependence on PKE in the 0–1 eV region,⁵⁶ it is unlikely that the 0–1 eV component can be assigned as $D_0 \leftarrow T_1$, which also corresponds to photoionization from a $\pi^*(2b_{3u})$ orbital. Therefore, the 0–1 eV component can be assigned as photoionization from vibrationally hot S_0 populated via cascaded IC of $S_2 \rightarrow S_1 \rightarrow S_0$ into D_0 . To confirm this assignment, we calculated the photoelectron anisotropy parameter for $D_0 \leftarrow S_0$ as a function of PKE using the same method as described in our previous theoretical study.⁵⁶ The calculation was performed for randomly oriented pyrazine molecules, in accord with the time averaging of β_2 from 50 to 80 ps. The calculated result is presented with a solid line in Fig. 8(b), which reasonably reproduces the flat PKE dependence with nearly zero values observed for 0–1 eV. This ensures that the 0–1 eV component originates from $D_0 \leftarrow S_0$ photoionization. The PKED for vibrationally cold S_0 taken as 6ω one-color signal is also presented with a dotted line in Fig. 8(a), demonstrating that the 0–1 eV

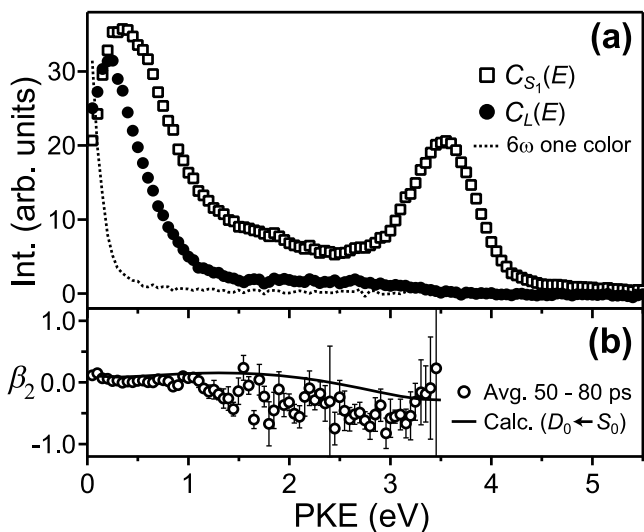


FIG. 8. (a) Coefficients, $C_{S_1}(E)$ and $C_L(E)$, obtained from the global fitting using Eq. (3). One-color PKED observed only with the 6ω probe pulse is also shown with a dotted line. (b) Photoelectron anisotropy parameter, β_2 , in Eq. (4) averaged from 50 to 80 ps as a function of PKE.

component (PKED for vibrationally hot S_0) is blue-shifted with respect to the dotted line owing to the vibrational excitation. As far as we know, this is the first real-time identification of vibrationally hot S_0 created by IC from an excited electronic state.

In addition to the 0–1 eV component, $C_L(E)$ exhibits a rather broad distribution with very small signal intensities in the PKE region of 1–3.5 eV. The β_2 parameters in the corresponding region have large uncertainties. As previously mentioned, Yamazaki *et al.*²⁴ estimated that the ISC quantum yield, Φ_{ISC} , to T_1 is 0.13 at the S_2 origin (264 nm). Therefore, the 1–3.5 eV component is likely due to photoionization signal from $T_1(n\pi^*, {}^3B_{3u})$ created by $S_2 \rightarrow S_1 \rightarrow T_1$ cascaded processes, to D_0 . In our previous TRPEI study on ISC from the S_1 origin, we revealed an isosbestic point in the time evolution of the PKEDs, indicating that the photoionization signals consist of two components, S_1 and T_1 , in dynamic equilibrium.³² However, such an isosbestic point should not be observed in the present study because of the reduced Φ_{ISC} (0.13), as seen in Fig. 8(a). In a previous study,³² T_1 was observed with a much lower (>1 eV) PKE than expected from the energy gap between the S_1 and T_1 origins (~0.5 eV).^{52,57} This is because the Franck-Condon factor between vibrationally hot T_1 and D_0 favors ionization into vibrationally excited states in D_0 . As seen in Fig. 8(a), the $D_0 \leftarrow T_1$ band is also observed with a much lower (>1 eV) PKE with respect to the $D_0 \leftarrow S_1$ band, consistent with the previous study.

To further check the formation of T_1 , we performed an additional experiment using (1 + 2') REMPI of $D_0 \leftarrow {}^1R(3s) \leftarrow S_1$ and $D_0 \leftarrow {}^3R(3s) \leftarrow T_1$, where ${}^1R(3s)$ and ${}^3R(3s)$ denote singlet and triplet 3s Rydberg states, respectively. The excitation scheme is schematically shown in Fig. 1(b). We have shown previously that the energy difference between ${}^1R(3s)$ and ${}^3R(3s)$ is 0.06 eV (484 cm^{-1}), and identified ISC from S_1 to T_1 using these transitions.⁵⁸ Thus, we employed the 264-nm pump pulses to create S_2 and 358-nm probe pulses to probe the subsequently populated S_1 and T_1 . Two-photon ionization from vibrationally hot S_0 with a 358-nm probe is energetically impossible. Fig. 9 presents

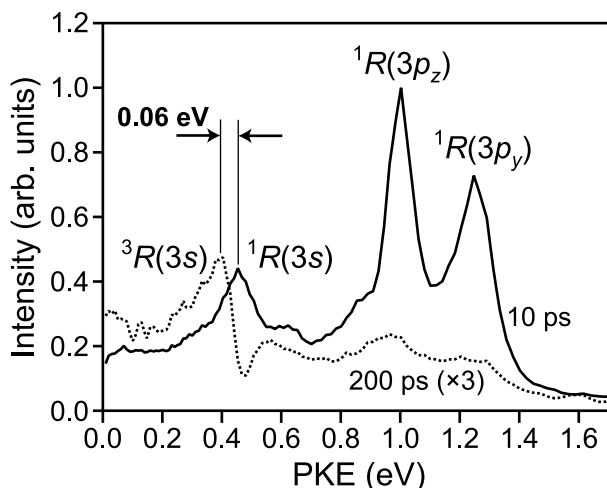
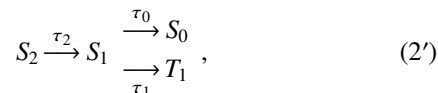


FIG. 9. PKEDs observed by (1 + 2') REMPI using 264-nm pump and 358-nm probe pulses at delay times of 10 ps (solid line) and 200 ps (dotted line).

PKEDs observed at pump-probe delay times of 10 ps (solid line) and 200 ps (dotted line) using the (1 + 2') REMPI scheme described above. At 10 ps, two-photon ionization occurs primarily from S_1 , and the three observed peaks are, respectively, assigned as photoionization via ${}^1R(3s)$, ${}^1R(3p_z)$, and ${}^1R(3p_y)$ Rydberg states in ascending order of PKE. At 200 ps, two-photon ionization occurs from T_1 and the ${}^3R(3s)$ peak has clearly shifted by -0.06 eV with respect to the ${}^1R(3s)$ peak observed at 10 ps, demonstrating that T_1 is actually created via $S_2 \rightarrow S_1 \rightarrow T_1$ cascaded radiationless transitions.

Because we have identified the long-lived components, vibrationally hot S_0 and T_1 , the model of sequential radiationless transitions (Eq. (2)) now has to be modified as follows:



where τ_0 and τ_1 are the lifetimes of the $S_1 \rightarrow S_0$ and $S_1 \rightarrow T_1$ radiationless decays, respectively. Rigorously speaking, radiative decay must be included in Eq. (2'); however, it was not taken into account in the present study because the radiative decay time is much (3–5 orders of magnitude) longer than τ_0 and τ_1 .²⁴ Consequently, the relationship between τ (14.8 ps) in Eq. (2) and τ_0 and τ_1 in Eq. (2') is $\tau^{-1} = \tau_0^{-1} + \tau_1^{-1}$.

As discussed earlier, the quantum yield of $S_2 \rightarrow S_1$ IC is considered to be unity, and thus the ISC quantum yield, Φ_{ISC} , can be expressed as follows:

$$\Phi_{\text{ISC}} = \frac{\tau_1^{-1}}{\tau_0^{-1} + \tau_1^{-1}} = \frac{\tau_1^{-1}}{\tau^{-1}}. \quad (5)$$

If we can evaluate the relative intensity between $D_0 \leftarrow S_0$ and $D_0 \leftarrow T_1$ photoionization signals, Φ_{ISC} may also be estimated from the PKEDs. However, such estimation was not attempted in this study, since the Franck-Condon envelope for $D_0 \leftarrow S_0$ photoionization was not fully observed, as shown in Fig. 8(a). Therefore, we used the value of Φ_{ISC} (0.13 at 264 nm) estimated by Yamazaki *et al.*²⁴ and calculated τ_0 and τ_1 using Eq. (5). The calculated values of τ_0 and τ_1 were 17 and 110 ps.

As mentioned earlier, the lifetime (14.8 ps) measured using the 3ω pump and 6ω probe pulses is slightly shorter than the value (17.5–22 ps) measured at around the S_2 origin (264 nm).^{24,28,29} To examine this difference in more detail, we measured τ as a function of excitation wavelength from 270 to 244 nm using (1 + 2') REMPI. One of the photoelectron intensity decay profiles observed at 260 nm is presented in Fig. 10(a). The profile is well explained by single exponential decay (dotted line) and rise (dashed line) functions with the same time constant of 13.4 ps. Similarly, we determined τ as a function of the excitation wavelength, as summarized in Fig. 10(b); the lifetime diminishes for shorter wavelengths from 270 to 244 nm. The spectrum of our 3ω pulse (dotted line) and a photoabsorption spectrum of pyrazine vapor measured at room temperature (solid line) are shown in Fig. 10(c). The most intense part of the 3ω spectrum is at 261 nm, where the value of τ (14.8 ps) agrees well with the values independently measured using (1 + 2') REMPI. Gordon *et al.*⁵⁹ recently

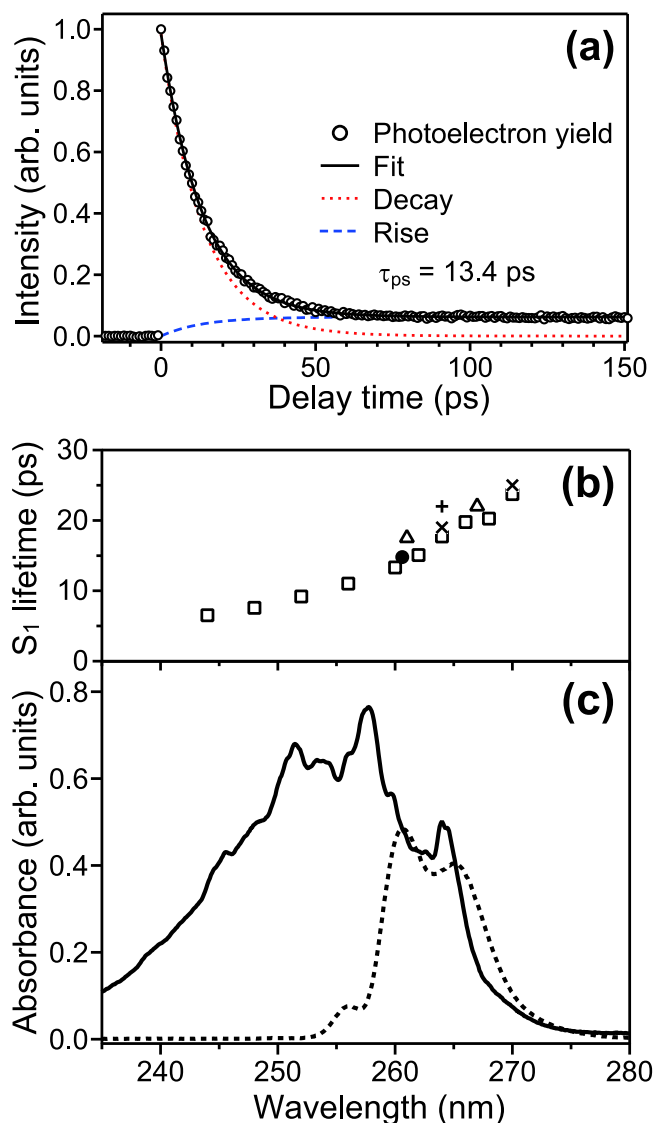


FIG. 10. (a) Photoelectron total yield as a function of the delay time between the 260-nm pump and 360-nm probe pulses using a $(1+2')$ REMPI scheme (see Fig. 1(b)). The observed signals are shown with open circles, while the fitting result is shown with a solid line. (b) The lifetime, τ , measured as a function of the excitation wavelength from 270 to 244 nm (\square). The other symbols correspond to the results obtained from the 3ω pump and 6ω probe experiment (\bullet) and those of previous investigations described in Refs. 24 (\times), 28 (+), and 29 (Δ). (c) Photoabsorption spectrum of pyrazine vapor at room temperature (solid line) overlaid with the 3ω spectrum (dotted line).

reported the lifetime to be 14.3 ± 0.2 ps at 261 nm, which is also in agreement with our result.

D. Time-energy map of photoelectron angular anisotropy

As our previous study using a 4ω probe pulse demonstrated,²⁶ time-dependent PADs reveal ultrafast IC from the S_2 state. Fig. 3(e) presents a time-energy map of β_2 measured in this study for early delay times of -47 to $+49$ fs. The β_2 values are presented only in the region where the normalized photoelectron intensities in Fig. 3(a) are greater than 0.1; β_2 values with smaller photoelectron intensities have large uncertainties, as shown in Fig. 8(b). As can be seen in

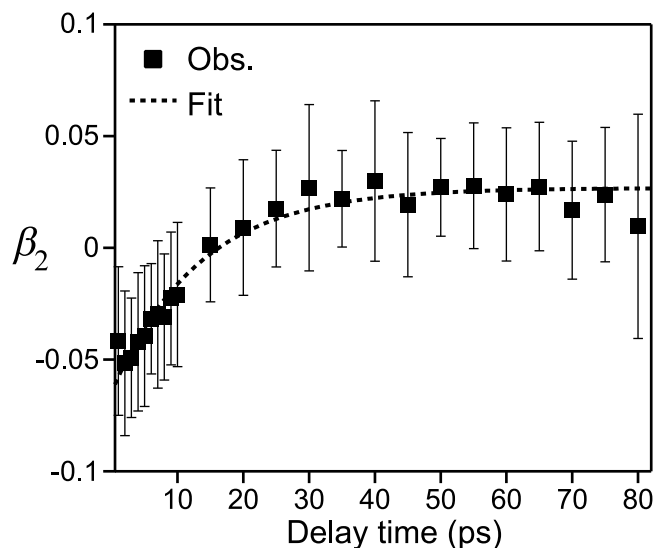


FIG. 11. Averaged β_2 values from 0.2 to 0.8 eV (solid squares). The fitting result using an exponential rise function, $a + b[1 - \exp(-t/\tau_{\text{beta}})]$, is also shown with a dotted line.

the PKE region from 3 to 4.5 eV in Fig. 3(e), the PAD of the S_2 state is almost isotropic ($\beta_2 \sim 0$), while formation of the S_1 state reduces β_2 , making the PAD anisotropic, with more photoelectrons emitted perpendicular to the laser polarization ($\beta_2 \sim -0.2$). It is noted that the β_2 values are different between the previous and present studies, as the anisotropy varies with the electron kinetic energy. A similar 2D map for β_4 revealed that the absolute values of β_4 were close to zero in the entire region. We also extracted β_2 parameters for longer time delays, as presented in Fig. 3(f). Close examination of β_2 in the PKE region from 0.2 to 0.8 eV revealed that β_2 gradually increases with the delay time, as shown in Fig. 11. The photoelectron signals in this PKE region are due to the photoionization processes $D_y \leftarrow S_1$ and $D_0 \leftarrow S_0$; therefore, the gradual increase of β_2 is ascribed to IC from S_1 to S_0 . We estimated the rate of change of β_2 in Fig. 11 using an exponential rise function of $a + b[1 - \exp(-t/\tau_{\text{beta}})]$. The fitting result is presented with a dotted line in Fig. 11 and the time constant, τ_{beta} , was determined to be 13 ± 8 ps, which is consistent with the value of 14.8 ps estimated from the photoelectron intensity decay profile.

IV. CONCLUSION

In this study, we demonstrated TRPEI using 9.3-eV probe (6ω) pulses as a single technique that enables observation of the entire cascaded electronic deactivation processes of photoexcited large molecules. The method has significant advantages over experiments using deep UV probe pulses. In the accompanying paper,⁶⁰ we note that 3ω -pump and 5ω -probe TRPEI on pyrazine suffered from a strong resonant transition to highly excited valence/Rydberg states by 5ω VUV pulses, while the present experiment using the 6ω probe pulses captured the deep-UV excited dynamics much more clearly. The time evolution of the PKEDs and PADs with the VUV universal ionization probe revealed the nuclear wavepacket motion from the S_2 Franck-Condon region to

the S_2/S_1 CI, the rapidly growing S_1 state via the CI, and the subsequent cascaded-radiationless transitions from the vibrationally hot S_1 state into S_0 and $T_1(n\pi^*)$. No signature of the $^1A_u(n\pi^*)$ dark state, which has been recently suggested by theoretical calculations as being involved in $S_2(\pi\pi^*) \rightarrow S_1(n\pi^*)$ decay,^{36,37} was observed. Configuration interaction of the $S_2(\pi\pi^*)$ electronic wave function was clearly observed via photoionization into multiple cationic states, demonstrating that TRPEI with VUV probe pulses provides an experimental method to explore the configuration interaction of electronic excited states.

It would be very interesting to apply this methodology to a variety of molecules, such as DNA bases, for which electronic relaxation down to the ground state is important for their functions. It is also interesting to explore how configuration interactions change when a photochemical reaction is accompanied by a large change in the molecular structure and conformation. Additionally, we are confident that the same approach coupled with a liquid microjet will open the door for elucidating complete non-adiabatic dynamics in solutions. Such an effort is currently in progress in our laboratory.

ACKNOWLEDGMENTS

This work was supported by JSPS KAKENHI Grant Nos. 15H05753 and 25620012. The authors thank Professor V. Bonačić-Koutecký, Professor T. J. Martinez, and Professor R. Mitrić for valuable discussions and Dr. M. Kanno for providing his results of multireference configuration interaction calculations. R.A.I. acknowledges JSPS Short Term Pre/Postdoctoral Fellowship for North American and European Researchers.

- ¹A. Stolow, A. E. Bragg, and D. M. Neumark, *Chem. Rev.* **104**, 1719 (2004).
- ²I. V. Hertel and W. Radloff, *Rep. Prog. Phys.* **69**, 1897 (2006).
- ³T. Suzuki, *Annu. Rev. Phys. Chem.* **57**, 555 (2006).
- ⁴T. Horio, R. Spesyvtsev, and T. Suzuki, *Opt. Express* **21**, 22423 (2013).
- ⁵T. Horio, R. Spesyvtsev, and T. Suzuki, *Opt. Lett.* **39**, 6021 (2014).
- ⁶A. L. Sobolewski, W. Domcke, C. Dedonder-Lardeux, and C. Jouvet, *Phys. Chem. Chem. Phys.* **4**, 1093 (2002).
- ⁷C. E. Crespo-Hernández, B. Cohen, P. M. Hare, and B. Kohler, *Chem. Rev.* **104**, 1977 (2004).
- ⁸D. Polli, P. Altoè, O. Weingart, K. M. Spillane, C. Manzoni, D. Brida, G. Tomasello, G. Orlandi, P. Kukura, R. A. Mathies, M. Garavelli, and G. Cerullo, *Nature* **467**, 440 (2010).
- ⁹M. Boggio-Pasqua, M. Ravaglia, M. J. Bearpark, M. Garavelli, and M. A. Robb, *J. Phys. Chem. A* **107**, 11139 (2003).
- ¹⁰H. J. Wörner, J. B. Bertrand, B. Fabre, J. Higuier, H. Ruf, A. Dubrouil, S. Patchkovskii, M. Spanner, Y. Mairesse, V. Blanchet, E. Mével, E. Constant, P. B. Corkum, and D. M. Villeneuve, *Science* **334**, 208 (2011).
- ¹¹W. Domcke, D. R. Yarkony, and H. Köppel, *Conical Intersections*, Advanced Series in Physical Chemistry Vol. 15 (World Scientific, Singapore, 2004).
- ¹²C. Woywod, W. Domcke, A. L. Sobolewski, and H. J. Werner, *J. Chem. Phys.* **100**, 1400 (1994).
- ¹³T. Gerdts and U. Manthe, *Chem. Phys. Lett.* **295**, 167 (1998).
- ¹⁴A. Raab, G. A. Worth, H.-D. Meyer, and L. S. Cederbaum, *J. Chem. Phys.* **110**, 936 (1999).
- ¹⁵M. Thoss, W. H. Miller, and G. Stock, *J. Chem. Phys.* **112**, 10282 (2000).
- ¹⁶C. Coletti and G. D. Billing, *Chem. Phys. Lett.* **368**, 289 (2003).
- ¹⁷R. Borrelli and A. Peluso, *J. Chem. Phys.* **119**, 8437 (2003).
- ¹⁸D. V. Shalashilin and M. S. Child, *J. Chem. Phys.* **121**, 3563 (2004).
- ¹⁹P. Puzari, R. S. Swathi, B. Sarkar, and S. Adhikari, *J. Chem. Phys.* **123**, 134317 (2005).
- ²⁰X. Chen and V. S. Batista, *J. Chem. Phys.* **125**, 124313 (2006).
- ²¹M. Barbatti, G. Granucci, M. Persico, M. Ruckebauer, M. Vazdar, M. Eckert-Maksić, and H. Lischka, *J. Photochem. Photobiol., A* **190**, 228 (2007).
- ²²U. Werner, R. Mitrić, T. Suzuki, and V. Bonačić-Koutecký, *Chem. Phys.* **349**, 319 (2008).
- ²³R. He, C. Zhu, C.-H. Chin, and S. H. Lin, *Chem. Phys. Lett.* **476**, 19 (2009).
- ²⁴I. Yamazaki, T. Mura, T. Yamanaka, and K. Yoshihara, *Faraday Discuss.* **75**, 395 (1983).
- ²⁵T. Fuji, T. Horio, and T. Suzuki, *Opt. Lett.* **32**, 2481 (2007).
- ²⁶T. Horio, T. Fuji, Y.-I. Suzuki, and T. Suzuki, *J. Am. Chem. Soc.* **131**, 10392 (2009).
- ²⁷Y.-I. Suzuki, T. Fuji, T. Horio, and T. Suzuki, *J. Chem. Phys.* **132**, 174302 (2010).
- ²⁸L. Wang, H. Kohguchi, and T. Suzuki, *Faraday Discuss.* **113**, 37 (1999).
- ²⁹V. Stert, P. Farmanara, and W. Radloff, *J. Chem. Phys.* **112**, 4460 (2000).
- ³⁰A. Frad, F. Lahmani, A. Tramer, and C. Tric, *J. Chem. Phys.* **60**, 4419 (1974).
- ³¹F. Lahmani, A. Tramer, and C. Tric, *J. Chem. Phys.* **60**, 4431 (1974).
- ³²T. Suzuki, in *Modern Trends in Chemical Reaction Dynamics, Part I: Experiment and Theory*, Advanced Series in Physical Chemistry Vol. 14, edited by X. Yang and K. Liu (World Scientific, Singapore, 2004).
- ³³T. Suzuki, *Int. Rev. Phys. Chem.* **31**, 265 (2012).
- ³⁴T. Suzuki, L. Wang, and H. Kohguchi, *J. Chem. Phys.* **111**, 4859 (1999).
- ³⁵S. Y. Liu, Y. Ogi, T. Fuji, K. Nishizawa, T. Horio, T. Mizuno, H. Kohguchi, M. Nagasono, T. Togashi, K. Tono, M. Yabashi, Y. Senba, H. Ohashi, H. Kimura, T. Ishikawa, and T. Suzuki, *Phys. Rev. A* **81**, 031403 (2010).
- ³⁶M. Sala, B. Lasorne, F. Gatti, and S. Guérin, *Phys. Chem. Chem. Phys.* **16**, 15957 (2014).
- ³⁷M. Sala, S. Guérin, and F. Gatti, *Phys. Chem. Chem. Phys.* **17**, 29518 (2015).
- ³⁸M. Kanno, Y. Ito, N. Shimakura, S. Koseki, H. Kono, and Y. Fujimura, *Phys. Chem. Chem. Phys.* **17**, 2012 (2015).
- ³⁹M. Schmitt, S. Lochbrunner, J. P. Shaffer, J. J. Larsen, M. Z. Zgierski, and A. Stolow, *J. Chem. Phys.* **114**, 1206 (2001).
- ⁴⁰Y.-I. Suzuki, T. Horio, T. Fuji, and T. Suzuki, *J. Chem. Phys.* **134**, 184313 (2011).
- ⁴¹U. Even, J. Jortner, D. Noy, N. Lavie, and C. Cossart-Magos, *J. Chem. Phys.* **112**, 8068 (2000).
- ⁴²A. T. J. B. Eppink and D. H. Parker, *Rev. Sci. Instrum.* **68**, 3477 (1997).
- ⁴³G. A. Garcia, L. Nahon, and I. Powis, *Rev. Sci. Instrum.* **75**, 4989 (2004).
- ⁴⁴M. Oku, Y. Hou, X. Xing, B. Reed, H. Xu, C. Chang, C. Y. Ng, K. Nishizawa, K. Ohshimo, and T. Suzuki, *J. Phys. Chem. A* **112**, 2293 (2008).
- ⁴⁵C.-K. Lin, Y. Niu, C. Zhu, Z. Shuai, and S. H. Lin, *Chem. - Asian J.* **6**, 2977 (2011).
- ⁴⁶M. Hackmeyer and J. L. Whitten, *J. Chem. Phys.* **54**, 3739 (1971).
- ⁴⁷C. Fridh, L. Åsbrink, B. Ö. Jonsson, and E. Lindholm, *Int. J. Mass Spectrom. Ion Phys.* **8**, 101 (1972).
- ⁴⁸W. von Niessen, W. P. Kraemer, and G. H. F. Dierksen, *Chem. Phys.* **41**, 113 (1979).
- ⁴⁹J. V. Ortiz and V. G. Zakrzewski, *J. Chem. Phys.* **105**, 2762 (1996).
- ⁵⁰D. M. P. Holland, A. W. Potts, L. Karlsson, M. Stener, and P. Decleva, *Chem. Phys.* **390**, 25 (2011).
- ⁵¹I. C. Walker and M. H. Palmer, *Chem. Phys.* **153**, 169 (1991).
- ⁵²Y. Udagawa, M. Ito, and I. Suzuka, *Chem. Phys.* **46**, 237 (1980).
- ⁵³See supplementary material at <http://dx.doi.org/10.1063/1.4955296> for the explicit analytical solutions.
- ⁵⁴E. T. Sevy, M. A. Muyskens, S. M. Rubin, G. W. Flynn, and J. T. Muckerman, *J. Chem. Phys.* **112**, 5829 (2000).
- ⁵⁵T. G. Dietz, M. A. Duncan, A. C. Pulu, and R. E. Smalley, *J. Phys. Chem.* **86**, 4026 (1982).
- ⁵⁶Y.-I. Suzuki and T. Suzuki, *J. Chem. Phys.* **137**, 194314 (2012).
- ⁵⁷J. L. Tomer, K. W. Holtzclaw, D. W. Pratt, and L. H. Spangler, *J. Chem. Phys.* **88**, 1528 (1988).
- ⁵⁸J. K. Song, M. Tsubouchi, and T. Suzuki, *J. Chem. Phys.* **115**, 8810 (2001).
- ⁵⁹R. J. Gordon, Z. Hu, T. Seideman, S. Singha, M. Sukharev, and Y. Zhao, *J. Chem. Phys.* **142**, 144311 (2015).
- ⁶⁰T. Horio, Y.-I. Suzuki, and T. Suzuki, *J. Chem. Phys.* **145**, 044307 (2016).